Evolution of active sites during selective oxidation of methane to methanol over Cu-CHA and Cu-MOR zeolites as monitored by operando XAS

Evolution of active sites during selective oxidation of methane to methanol over Cu-CHA and Cu-MOR zeolites as monitored by operando XAS

Elisa Borfecchia[1,2], Dimitrios K. Pappas[3], Michael Dyballa[3], Kirill A. Lomachenko[4], Chiara Negri[1], Matteo Signorile[1], Gloria Berlier[1*]

[1]Department of Chemistry and INSTM Reference Center, University of Turin, via P. Giuria 7, 10125 Turin (Italy)

[2]Haldor Topsøe A/S, Haldor Topsøes Allé 1, 2800 Kongens Lyngby (Denmark)

[3]Center for Materials Science and Nanotechnology (SMN), Department of Chemistry, University of Oslo, 1033 Blindern, 0315 Oslo (Norway)

[4]European Synchrotron Radiation Facility (ESRF), 71 avenue des Martyrs, CS 40220, 38043 Grenoble Cedex 9, France

The local structural and electronic properties of Cu sites during the direct conversion of methane to methanol with molecular oxygen was followed by X-ray absorption spectroscopy (XAS) on a set of Cu-zeolites with different topology (large pore MOR and small pore CHA frameworks) and similar chemical composition (Si/Al ~ 11 and 12, respectively). Two low loading (LL) and high loading (HL) samples were prepared by ion exchange, and their methanol productivity measured in laboratory fixed bed reactor tests, resulting in selectivity higher than 85%. Both Cu-MOR samples outperformed Cu-CHA ones, resulting in 0.28 and 0.26 molCH_3OH/molCu for the LL (Cu/Al = 0.13) and HL (Cu/Al = 0.36) samples, *vs* 0.10 and 0.17 molCH_3OH/molCu for LL and HL Cu-CHA, respectively (Cu/Al = 0.16 and 0.49). The evolution of Cu oxidation state and local coordination environment was followed in all the reaction steps (O_2 activation, flush with He, CH_4 dosage and subsequent CH_3OH desorption by applying a wet stream) both during temperature changes (ramp in O_2 up to 500 °C, cooling to 200 °C for subsequent steps, etc.) and in steady-state conditions. Strong similarities were observed in the local structure of Cu sites in all samples, which showed similar redox dynamics during O_2 activation and subsequent cooling to 200 °C. Even though only qualitative considerations can be made on the overall spectral evolution, XANES indicates that not all the Cu(I) formed during CH_4 loading belongs to active sites.

Keywords
XAS spectroscopy, EXAFS, XANES, Cu-CHA, methane to methanol

1 Introduction

Since from the first report by Groothaert et al. about the possibility to obtain methanol by direct oxidation of methane with molecular oxygen on Cu-ZSM-5 and Cu-MOR zeolites [17], a lively debate has appeared in the literature about the nature of the involved Cu sites and the possibility to develop strategies for an industrially-viable process. Indeed, the direct conversion of methane to methanol (MTM) is a so-called 'dream reaction' in relation to the chemical inertness of the reactant and intrinsic reactivity of the product. In fact, C–H bond energy in methane is the highest among hydrocarbons (413 kJ mol^{-1}), while methanol is characterized by a significant dipole moment which implies a facile interaction with the catalyst active sites, favouring over-oxidation reactions. On the other hand, processes based on the direct route have a tremendous economic and environmental appeal, in relation to the large availability of methane in natural gas sources, and to the huge amount flared or vented into the atmosphere, mainly at oil extraction sites (approximately 1/3 of the annual methane consumption of Europe, according to recent estimates). On the contrary, methanol is an important feedstock for the chemical industry (more than 48 million tonnes produced yearly [37]) and being liquid does not present the safety and economic issues related to transport and storage of gaseous methane. The possibility to design a catalyst and a process for the direct MTM reaction on-site (where methane is naturally abundant) thus represents an intriguing challenge for the scientific community.

Very recently, Prof. van Bokhoven and coworkers proposed the possibility to carry out MTM over Cu-zeolites in anaerobic conditions, using water as oxidizing agent [50]. This approach is aimed at overcoming the limitations of the stepwise reaction with molecular oxygen, which requires activation at high temperature, reaction with methane at lower temperature and methanol extraction from the catalyst surface by a wet stream. Another limitation of the reaction is the low productivity, with the highest reported values of 0.35 mol_{CH3OH}/mol_{Cu} (160 μmol/g) on Cu-MOR [19, 20], followed by 0.2 mol_{CH3OH}/mol_{Cu} on Cu-ZSM-5 [35] and Cu-SSZ-13 [42]. Concerning Cu-SSZ-13, this is a small pore CHA zeolite, which was reported to be active in the MTM reaction with molecular oxygen only recently, with lower methanol productivity ($0.03 - 0.09$ mol_{CH3OH}/mol_{Cu}) [56] with respect to the most studied medium and large pore zeolites (MFI and MOR). The better performance mentioned above was obtained by Pappas et al. on a sample with Si/Al = 12 and Cu/Al = 0.5, by optimizing the pre-treatment and reaction steps conditions (time and temperature, O_2 and CH_4 partial pressures) [42].

A different approach for the 'dream reaction' was recently proposed by Hutchings' group, who carried out methane oxidation in aqueous medium with Fe-zeolites in the presence of H_2O_2 [23]. In this case active catalysts were shown to be Fe-silicalite samples, where iron was introduced during the synthesis as framework heteroatoms. These form highly dispersed extraframework sites upon calcination, similarly to what observed for Fe-zeolites active in the N_2O-mediated selective oxidation of methane and benzene [8,Dubkov, 2002 #379, 39,Panov, 1998 #376]. However, XANES and DR UV-Vis spectroscopy studies pointed to the role of Fe(III) as active sites in the H_2O_2-based catalysis [21], at variance with the so-called Fe(II) α-sites, able to decompose N_2O to form the active α-oxygen [11, 39,Panov, 1998 #376]. The reaction was proposed to involve a bis(μ-hydroxo)diiron complex with formula $[Fe_2(\mu_2\text{-}OH)_2(OH)_2(H_2O)_2]^{II}$, containing antiferromagnetically coupled high-spin octahedral Fe(III) centers. H_2O_2 coordination to one Fe(III) atom would result in a Fe(IV)/Fe(II) dimer with a hydroperoxy ligand adsorbed on the Fe(IV) atom, and formation of a ferryl Fe(IV)=O upon coordination of a second H_2O_2 molecule. Insertion of Cu(II) ions in Fe-zeolites was instead reported to increase selectivity, by suppressing overoxidation reactions due to $^{\bullet}OH$ radicals [23].

An important challenge for this kind of catalyst is about increasing active sites dispersion, by reducing the well-known tendency of iron towards agglomeration. This issue was addressed by isomorphous framework substitution of trivalent non-catalytically active atoms, namely Al(III) and Ga(III)) [22], or by heat treating in hydrogen before calcination samples prepared by chemical vapour impregnation, to reduce the amount of available oxygen in the micropores and thus limit agglomeration [12]. In the latter example, the authors pointed to the importance of isolated octahedral extraframework iron-oxo clusters and/or Fe(II) sites in directing high selectivity to alcohols, also in the absence of Cu(II) as $^{\bullet}OH$ radical scavengers [12]. Finally, resonance Raman

studies of Fe-silicalite and Fe-ZSM-5 suggested a reversible shift between the bis(μ-hydroxo)diiron complex and two transient mononuclear Fe(III)-OOH sites, formed in the presence of H_2O_2 [24].
Coming back to Cu-zeolites, apart from the efforts to improve the process design to move from a fascinating scientific playground to a viable industrial process, most of the last decade literature has been focused on the determination of the active sites electronic and geometric structure. The first reports on medium pore Cu-ZSM-5 pointed to the presence of dinuclear Cu sites, able to activate O_2 with the formation of a bent Cu(II) mono(μ-oxo)dicopper core [55]. This was proposed to be responsible for the typical UV-Vis band at 22700 cm^{-1} (disappearing upon CH_4 contact [17],) and for the resonance Raman (rR) bands at 456, 870 and 1725 cm^{-1}, moving to 448, 830 and 1642 cm^{-1} upon isotope exchange with $^{18}O_2$ [55]. A very similar structure was proposed to be present in Cu-MOR (UV-Vis fingerprint at 22200 cm^{-1} and rR bands at 450, 850, 1700 and 1850 cm^{-1}) [53]. DFT calculations resulted in a very similar geometry of the dinuclear core for both topologies, implying a similar structural motif in the two frameworks, with Al framework atoms (Al_{fw}, each generating a negative charge) at 7.5 Å [53]. Namely, activation of O_2 was found to be favoured by a pair of Cu(I) ions at a distance around 4.2 Å, located at the intersection of straight and sinusoidal 10-membered rings (10r) in MFI [52] and at the intersection of the side pocket with the 12r and 8r channel in MOR [53].
The presence of these active dinuclear cores in Cu-MOR was not questioned in the X-ray Absorption Spectroscopy (XAS) studies by Prof. van Bokhoven and coworkers, who however proposed the presence of a significant fraction of not precisely described active 'Cu(II)-O like' species [3]. Moreover, the same group observed by TEM the presence of finely dispersed nanoparticles (≤ 3 nm), which were proposed to be active after activation in O_2 at low temperature (200 °C), in the presence of high methane pressure (36-50 bar) [51]. As acknowledged by the authors, these findings point to the fact that XAS data need to be analysed with great care when the studied system is not a 'single site' catalysts, due to the fact that it averages all Cu sites present in the sample. On the other hand, Grundner et al. used this technique to characterize Cu-MOR samples prepared by a controlled ion exchange protocol, minimizing copper hydrolysis and precipitation and the competition from alkaline cations [20]. The authors observed a correlation between methanol productivity and Cu content in a series of Cu-MOR with different Si/Al ratios, with a slope of 0.33, suggesting that three Cu atoms are needed to convert one methane molecule to methanol. Thus XAS data were interpreted in terms of the presence of 'single site' tris(μ-oxo)tricopper $[Cu_3(\mu\text{-}O)_3]^{II}$ complexes located at the entrance of the MOR side pocket, as supported by DFT calculations [20].
This contribution is thus set within the intriguing debate about the nature of the Cu sites responsible for activation of molecular oxygen, and on the resulting Cu-oxo structure and nuclearity. More in detail, we have studied by XANES and EXAFS the evolution of Cu sites during the MTM process steps (O_2 activation and subsequent He flush, CH_4 interaction and CH_3OH desorption in a wet stream) on a set of low and high loading Cu-CHA and Cu-MOR samples with similar Si/Al and Cu/Al ratios, trying to underpin the effect of zeolite topology and chemical composition on Cu speciation. The changes in the oxidation state and local geometry of copper sites have been followed both dynamically (*i.e.* during the ramp in O_2 for activation, while decreasing temperature before CH_4 interaction, and at increasing interaction time with CH_4 and H_2O) and in steady-state conditions. The catalytic activity of the same set of samples was measured in two series of separate experiments, one using the parameters optimized by Pappas et al. to obtain the highest productivity [42], and one with the shorter timescale necessary for synchrotron experiments. The reported results only allow for qualitative considerations, not conclusive about the origin of the highest productivity of Cu-MOR, and about a precise description of the active Cu-oxo sites formed in the two different frameworks. However, they compare productivity and spectroscopic data obtained on a series of samples prepared and studied in exactly the same conditions, pawing the pay to further studies with more advanced data analysis, such as Principal Component Analysis (PCA) and Multivariate Curve Resolution (MCR) techniques.

2 Materials and Methods

2.1 Samples synthesis and compositional characteristics

H-CHA parent zeolite (Si/Al ~ 12) was synthesized according to the procedure described in a previous study [26]. A commercial NH_4-MOR (Si/Al ~ 11, Zeolyst Inc.) was twice ion-exchanged with NH_4NO_3 (10 wt% in water) at 60 °C for 5 h and washed NO_3-free. After drying, ammonia was burned off by heating in air at 500 °C for 8 h (1 °C /min heating ramp). Cu-zeolites were prepared by aqueous ion exchange using the necessary amount of copper(II) acetate (Sigma-Aldrich, 99.99%, 150 g water per 1 g of zeolite). The exchange was carried out under stirring at room temperature (RT) overnight at a pH adjusted to 5.2−5.7. After exchange, the material was washed thrice with water, filtered and dried at 50 °C.
The composition of the investigated samples, determined via Energy Dispersive X-Ray Spectroscopy (EDS), is reported in Table 1. The dispersion of Cu ions as well as the absence of large aggregates were confirmed by Scanning Electron Microscopy (SEM) and X-Ray Diffraction (XRD).

Table 1. Chemical composition of the investigated low loading (LL) and high loading (HL) Cu-CHA and Cu-MOR samples.

Sample Identification	Si/Al	Cu/Al	Cu wt%
LL Cu-CHA	12.1	0.16	1.2
HL Cu-CHA	12.1	0.49	3.8
LL Cu-MOR	11.3	0.13	1.1
HL Cu-MOR	11.3	0.36	3.1

2.2 Testing conditions

The investigated Cu-zeolites were tested for the stepwise MTM conversion in a quartz plug flow reactor of 6 mm internal diameter, using 100 mg of pelletized samples (425 to 250 μm). The reactor was heated with a tubular oven, with a thermocouple inserted in a capillary quartz tube in the middle of the Cu-zeolite bed for temperature control.
Initially, the material was kept at 150 °C in a He flow of 15 ml/min. A flow of 15 ml/min O_2 was then introduced and the temperature increased with a rate of 5 °C/min to 500 °C, where the sample stayed for 480 min (**O_2-activation** step). The sample was then cooled down to 200 °C, with the same rate of 5 °C/min in O_2, purged with He for 60 min, and then contacted with a 15 ml/min CH_4 flow for 360 min at 200 °C (**CH_4 loading** step). The **CH_3OH extraction** step was then carried out with a He wet flow (10% H_2O,15 ml/min), after flushing with dry He. A summary of the adopted conditions can be found in SI, Table S1. A Hewlett Packard 6890/5972 GCMS System was used to quantify the extracted products during the final step. The reaction yield was calculated considering the oxidized (i.e. methanol and dimethyl ether, accounted as two methanol molecules) and over-oxidized products (CO_x species). For a better comparison with the XAS results, the reported productivity is normalized per Cu (in molCH_3OH/molCu, Table S2), and is also reported as μmol/gcat in the product distribution plot (Figure S1).
The samples were also tested in a fixed bed reactor with a protocol simulating the conditions used for the XAS measurements (see below, Tables S3 and S4 in the SI and related discussion in Section 3.1).

2.3 XAS

Cu K-edge X-ray Absorption Spectroscopy (XAS) measurements were performed at the BM26A beamline [36] of the ESRF. XAS data collection was performed in transmission mode, using a Si (111) monochromator for the incident energy scan and ionization chambers for the detection of incident (I_0) and transmitted (I_1) photons. The powdered samples were prepared in the form of self-supporting pellets of optimized thickness and fixed inside a Microtomo reactor cell [6] equipped with a gas flow-set-up. Sample masses were in the 100-140 mg range for 1.3 cm^2 area pellets, depending on the composition, resulting in a total absorption after the edge of $\mu x = 2.5$ and edge jumps of $\Delta\mu x$ of 0.6-0.7 and 0.2-0.3 for high-loading and low-loading samples, respectively.
The protocol adopted for XAS experiment is schemed in SI, Figure S2. We applied the same temperature and gas conditions used in plug flow reactor laboratory tests to obtain the optimal performance. However, due to

time constraints during synchrotron experiments, time exposure to O_2 and CH_4 was reduced (180 min vs 480 min and 200 min *vs* 360 min, respectively). We have then used the same conditions to measure the samples productivity in independent fixed bed laboratory tests (Tables S3 and S4 in the SI and related discussion in Section 3.1). A fast acquisition mode was used to monitor the evolution of the XAS features during each process step. A higher-quality acquisition mode was employed to characterize the samples in steady-state conditions. Scan details for the two kind of measurements can be found in the SI (Section 2).
All the collected XAS spectra were normalized to unity edge jump employing the Athena software from the Demeter package [44]; the $\chi(k)$ functions were extracted with the same software. Fourier Transformed (FT) EXAFS spectra were obtained transforming the $k^2\chi(k)$ EXAFS functions in the (2.4 – 9.7) $Å^{-1}$ and (2.4 – 12.4) $Å^{-1}$ k-ranges for lower quality (evolution monitoring) and higher quality (steady-state conditions) scans, respectively.

3 Results and Discussion

3.1 Performance of the investigated Cu-zeolites for the MTM conversion

The normalized productivity in molCH_3OH/molCu (left axis) and selectivity (%) (right axis) of the tested Cu-CHA and Cu-MOR samples are depicted in Figure 1. The samples were tested for the stepwise MTM conversion utilizing conditions which maximise the methanol yield, that is long time exposure to O_2 and CH_4. All the materials convert methane to methanol with high selectivity (above 85%, see Figure S1 in the SI for an analysis of the products distribution) through the stepwise process, and more than 10% of copper is participating in the reaction. Cu-MOR materials produce 0.28 and 0.26 molCH_3OH/molCu for the LL (Cu/Al = 0.13) and HL (Cu/Al = 0.36) sample, respectively. In the case of Cu-CHA a higher discrepancy between the two different loadings, namely LL (Cu/Al = 0.16) and HL (Cu/Al = 0.49), is observed. The LL Cu-CHA produces 0.10 molCH_3OH/molCu while the HL Cu-CHA 0.17 molCH_3OH/molCu. This different performance is attributed to the existence of *2Al* Z_2Cu(II) sites in six-membered ring (6r) of the CHA framework (where Z_2 indicates bonds to O_{fw} next to two neighbouring charge-balancing Al sites in framework T-sites), proposed to be inactive for the conversion [25, 42]. The preferential initial population of these sites [4, 14, 41] together with their proven inactivity provide a reliable rational for the worse performance of LL Cu-CHA in comparison with HL Cu-CHA. On the other hand, the Cu-MOR samples show smaller difference between the two Cu loadings, indicating a more uniform distribution of Cu as active sites [19, 20], which have been proposed to be located in the eight-membered ring (8r) side pocket of the MOR structure [20, 50]. Comparing the performance of the two different Cu-exchanged zeolites, it is evident that Cu-MOR samples possess a higher fraction of active Cu sites allowing them to produce more CH_3OH per Cu.
In order to assess how the materials perform under the conditions applied for XAS measurements, the corresponding catalysts were also tested in a fixed bed reactor according to the XAS protocol. The results of these tests can be found in Table S4 in the SI. The measured productivities were lower for all the samples: as already observed [42], a shorter O_2 activation and CH_4 loading time result in a decrease of the productivity. The decrease observed is in the range of 30 to 50 %, more evident for the low-loading materials, while selectivity is not significantly affected by these parameters. On the other hand, the behavior of the materials exhibits very similar trend as described above with the Cu-MOR materials outperforming the corresponding Cu-CHA.

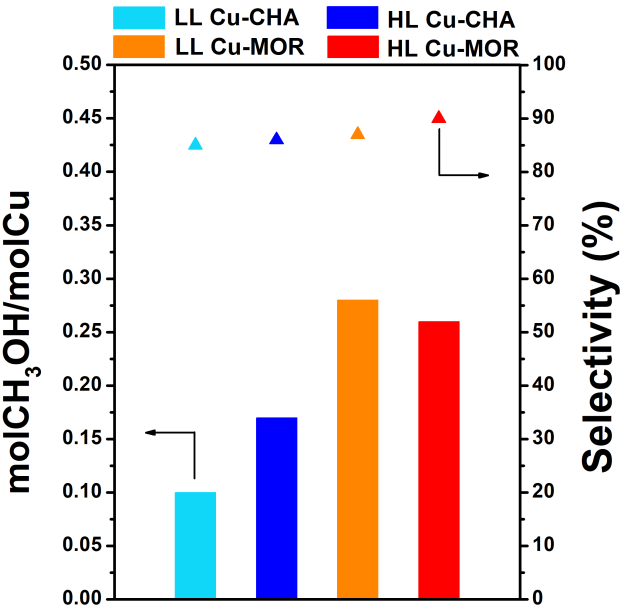

Figure 1. Normalized productivity in molCH$_3$OH/molCu (bars, left axis) and selectivity (%) (triangles, right axis) of Cu-CHA and Cu-MOR materials with different compositional characteristics, evaluated utilizing the process conditions summarized in the SI, Table S1.

3.2 Comparative overview of Cu-CHA and Cu-MOR at key process steps from XAS

We will initially focus on the analysis of the XAS spectra collected under steady-state conditions at the end of the key steps of the MTM process, to highlight general trends in the average electronic and structural properties of the Cu species formed as a function of Cu-loading and zeolite topology. With this respect, Figure 2 compares the four investigated samples in the XANES region. It is evident that the XAS spectra at each process step show rather similar features, reflecting a similar local coordination environment of the formed Cu-species. The characteristic XANES features can be interpreted following the abundant literature on Cu K-edge XANES in Cu-zeolites [2, 9, 15, 18, 29, 41, 42] and biological systems [27, 46, 49].

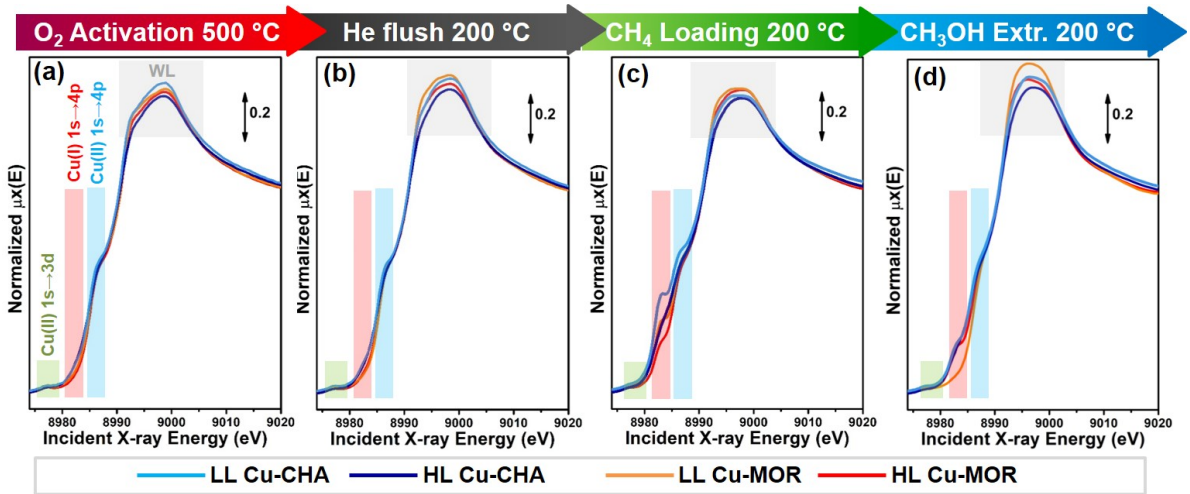

Figure 2. Cu K-edge XANES spectra of the investigated materials under steady-state conditions (a) at the end of the O_2 activation step at 500 °C, (b) at 200 °C in He, after the O_2-activation step and subsequent cooling down in O_2; (c) at 200 °C at the end of the CH_4 loading step; (d) at 200 °C at the end of the CH_3OH extraction step. The typical energy ranges for the key XANES fingerprints are highlighted by coloured boxes: green - Cu(II) 1s → 3d pre-edge peak; red - Cu(I) 1s → 4p rising-edge peaks (not observed here); blue - Cu(II) 1s → 4p rising-edge peaks; grey - "white-line" (WL) feature.

In line with a recent study for the HL Cu-CHA sample [42], at the end of the O_2 Activation step, Cu ions exist in a virtually total Cu(II) state for all the investigated materials (Figure 2a). A well-defined rising-edge peak

is always observed at 8986 eV (blue boxes in Figure 2), in the typical energy range of 1s → 4p transitions in trigonal planar Cu(II) centres. Conversely, the same transitions expected for Cu(I) ions are not observed (red boxes). The presence of the dipole-forbidden pre-edge peak mostly deriving from the 1s → 3d transition (green boxes) is another confirmation of the largely dominant presence of Cu(II) ions. Although in the pre-edge and edge-region the XANES spectra for all the probed Cu-zeolites are almost overlapped, we observe differences in the intensity and shape of the 'white line (WL) feature, peaking at ~ 8999 eV. WL intensity follows the order: LL Cu-CHA > LL Cu-MOR > HL Cu-MOR > HL Cu-CHA, suggesting topology- and Cu loading-induced differences in the average first-shell coordination number and/or geometry of the Cu(II) species formed during the O_2 activation step. The higher WL observed in the XANES of LL Cu-CHA is consistent with the presence of a higher fraction of Z_2Cu^{II} species in six-member ring (6r) *2Al* sites [9, 33, 41].

After O_2 activation, the samples are cooled down to 200 °C in O_2 and then flushed with He for 90 min (Figure 2b). Here, all the XANES fingerprints still support a largely dominant Cu(II) state. This points to the fact that He flush at 200 °C does not produces significant modifications in the average Cu oxidation state. An increase in the WL intensity with respect to the O_2-activated state at 500 °C is however observed for all the samples, pointing to a perturbation in the Cu coordination environment.

At the end of the CH_4 loading step (Figure 2c), we observe the decrease of the WL intensity and the development of a rising-edge peak at 8983 eV, in an energy range typical of Cu(I) 1s →4p transitions. In line with previous reports on both Cu-CHA [42] and Cu-MOR [3, 20], these are clear evidences of the formation of Cu(I), through partial reduction of the Cu(II) species formed during the O_2 activation step. In parallel, with respect to the previous state, the 1s→ 3d peak undergoes an intensity decrease for all samples. After H_2O-assisted CH_3OH extraction step (Figure 2d), XANES reveals the partial hydration of Cu ions, through the formation of mobile Cu(II) aquo-complexes. Comparing the XANES spectra to the CH_4-activation step, we see a shape change and an intensity increase of the white line, in agreement with the XAS signature of pseudo-octahedral Cu(II) aquo complexes. The Cu(I) characteristic peak at around 8983 eV is always diminished, and it completely disappears for LL Cu-MOR.

The FT-EXAFS spectra of the investigated samples are also very similar and undergoes comparable modifications along the MTM process (Figure 3a-d). Three peaks, corresponding to three different coordination shells around the Cu-centres, are always recognizable. Based on previous studies[42], we built up a simple fitting model to quantify, in a first approximation, the average structural parameters of the Cu species formed during the reaction steps (Figure 3e). The model includes a first shell of framework and extra-framework oxygen neighbours O_{fw+ef}. These two contributions cannot discriminated due to excessively high correlations of the sub-shells. A second shell is consistent with the presence of framework Al/Si atoms (T_{fw}), and a third-shell with a Cu···Cu_{ef} contribution. Further details on the fitting model and procedure can be found in SI, Section 4.

Notably, the interpretation of the second-shell peak is not straightforward. Previous EXAFS studies on Cu-CHA have connected this EXAFS feature with single shell (SS) paths involving T_{fw} atoms [31, 40], in very good agreement with DFT-optimized models of framework-interacting Cu-species formed at *1Al* and *2Al* framework sites [9, 33]. Conversely, in Cu-ZSM-5 [18] and in Cu-MOR [1] the well-defined second-shell peak observed in O_2-activated materials has been modelled with Cu···Cu SS paths in multinuclear moieties, such as Z[Cu_2(μ-O)]Z [1] and Z[Cu_3(μ-$O)_3$]Z clusters [20] (where Z indicates bonds to charge-balancing O_{fw} next to one Al in a framework T-sites).

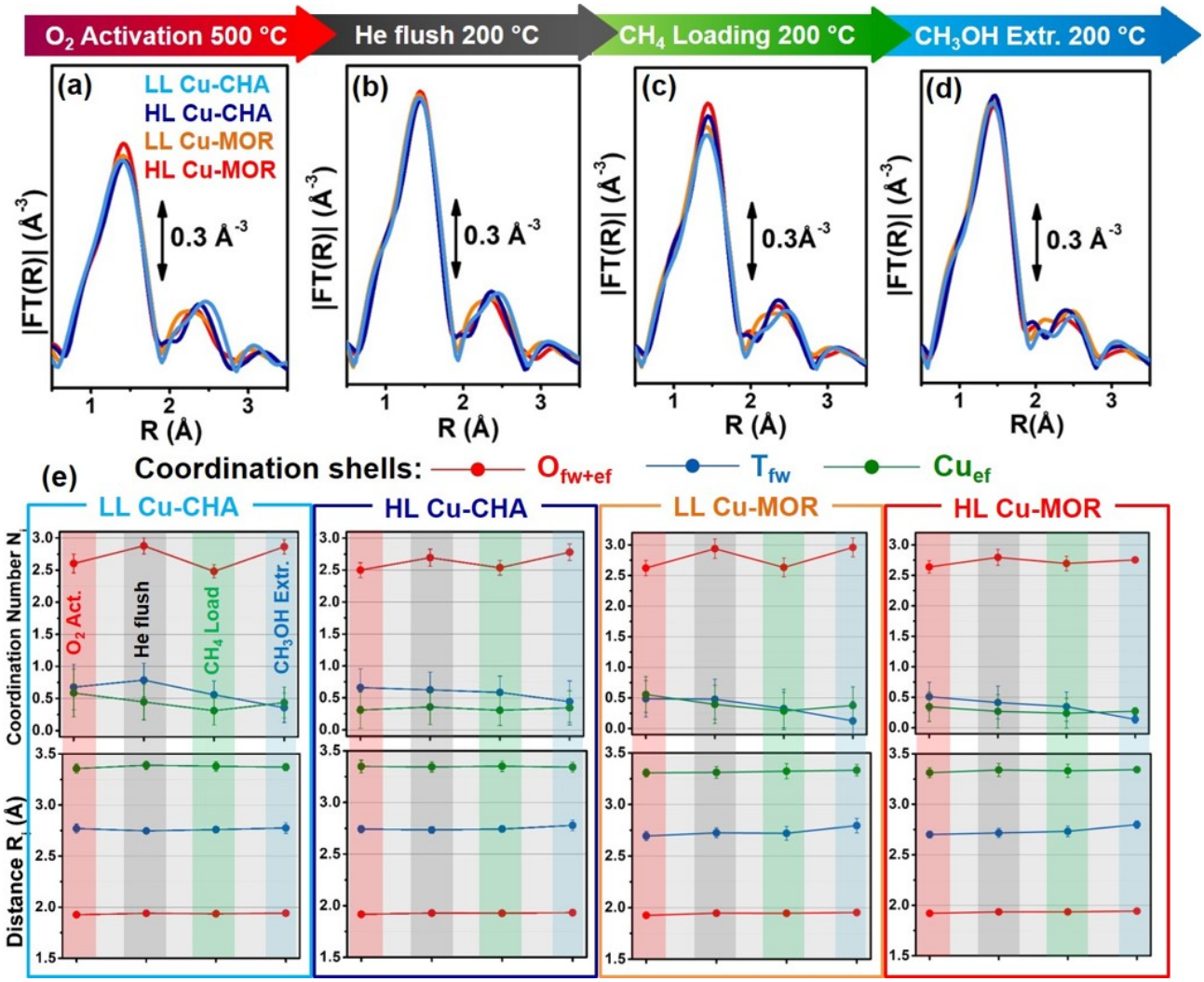

Figure 3. (a-d) Magnitude of the FT-EXAFS spectra obtained under steady-state conditions (a) at the end of the O_2 activation step at 500 °C, (b) at 200 °C in He, after cooling down in O_2; (c) at 200 °C at the end of the CH_4 Loading step; (d) at 200 °C at the end of the CH_3OH extraction step. (a) Structural parameters (average coordination numbers, N_i and bond distances R_i) obtained from EXAFS fitting of the spectra reported in parts (a-d).

We note that Cu-MOR and Cu-CHA materials, probed in the same conditions, show very similar EXAFS signatures in this R-space range (see also Figure S3, reporting a magnification of the magnitude and imaginary part of the FT-EXAFS spectra of interest in the second- and third-shell region). A good fit (R-factor < 2%, see SI) was obtained for all samples considering Cu···T_{fw} SS paths (expected to be present in both mono- and multi-copper species docked to the zeolite framework) and long-range Cu···Cu_{ef} paths (~3.3 Å, third-shell maximum). However, the presence of shorter Cu···Cu contributions (~2.8 Å), overlapped with the second-shell Cu···T_{fw} paths, cannot be excluded. Indeed, test fits performed including both contributions resulted in correlations up to 0.99 among the refined parameters, yielding unphysical optimized values and hindering their discrimination with conventional EXAFS analysis (see SI, Section 4.1). With this respect, further studies are ongoing exploring the potential of wavelet transform approaches [13, 34].

EXAFS analysis of O_2-activated materials evidences average coordination numbers of $N_{O(fw+ef)}$ ~ 2.6, and $N_{T(fw)}$ ~ 0.6, consistent with a major contribution from trigonal planar Cu species at *1Al* sites, showing slightly asymmetric ligation to O_{fw} and O_{ef} atoms. LL-Cu-CHA has slightly higher coordination numbers in both the first and the second shell ($N_{O(fw+ef)}$ = 2.6 ± 0.1; $N_{T(fw)}$ = 0.7 ± 0.3), together with a longer Cu-T_{fw} distance of 2.78 ± 0.04 Å, with respect to HL-Cu-CHA ($N_{O(fw+ef)}$ = 2.5 ± 0.1; $N_{T(fw)}$ = 0.6 ± 0.3; Cu-T_{fw} distance = 2.74 ± 0.04 Å). In agreement with the higher intensity of the WL observed in the XANES of LL Cu-CHA, this is

consistent with the presence of a higher fraction of Z_2Cu^{II} species in six-member ring (6r) *2Al* sites [9, 33, 41], completely inactive for the MTM conversion [42].
Following the He-flush at 200 °C, the intensity of the first-shell peak in the FT-EXAFS spectra is enhanced, resulting on average in $N_{O(fw+ef)} \sim 2.8$, indicating thermally-induced modifications in the Cu-coordination environment. This point will be addressed in more detail in the following (Section 3.4). After CH_4 loading, in concomitance with the detection of Cu(I) from XANES, the first shell coordination number diminishes in all the investigated materials, returning to $N_{O(fw+ef)} \sim 2.6$. The coordination number decrease is more pronounced for LL materials, where also $N_{T(fw)}$ and $N_{Cu(ef)}$ lowers by about 30% with respect to what observed in He prior to interaction with CH_4. Finally, after stream admission, EXAFS strongly supports partial hydration and mobilization of Cu ions. $N_{O(fw+ef)}$ increases again to 2.8, while an important decrease in $N_{T(fw)}$ is observed for all the samples, by 30% and 60% for Cu-CHA and Cu-MOR, respectively, with respect to the values observed upon interaction with CH_4.

3.3 Redox dynamics during the O_2 activation step

The O_2 activation step is a crucial one, resulting into the formation of the Cu active sites for the MTM conversion [48, 55]. Although it is well known that different activation conditions can drastically impact the material productivity (and thus the fraction of active *vs* inactive Cu species) [42], the pathways leading to the methane-converting Cu species are still debated.
While using XAS to monitor the MTM reaction, we observed for both Cu-CHA and Cu-MOR materials a peculiar redox behaviour during the O_2 activation step. Figure 4 reports the XANES evolution for a representative sample (LL Cu-CHA) while heating in O_2 from RT to 500 °C and waiting at 500 °C for 1 h, always in O_2 flow.
In the first part of the thermal treatment, together with the typical spectroscopic fingerprints associated with the transition from hydrated to framework-interacting Cu(II) species (i.e. decrease of the WL intensity, development of the rising-edge peak at 8986 eV), we also note the progressive development of the peak at 8983 eV characteristic of Cu(I) (Figure 4a). This behaviour is similar to the well-documented "self-reduction", occurring during thermal treatment of Cu-zeolites in inert gas flow or in vacuum and associated with the homolytic cleavage of the Cu−OH bond in Z[Cu(II)OH] moieties [9, 30, 33, 38].
Thus, even in pure O_2, we detect the transient development of Cu(I) species. However, from 350 °C upwards the Cu(I) peak starts to progressively decrease, resulting in a virtually total Cu(II) state once 500 °C is reached (Figure 4b). As evidenced in Figure 4c, we observed the same "transient reduction" phenomenon for all the monitored Cu-zeolites. The intensity of the Cu(I) peak is higher for Cu-MOR: this can indicate either a higher fraction of transiently reduced Cu species in MOR or a more linear coordination geometry for such species, resulting into an intensity enhancement for the 1s → 4p peak. If Cu-zeolites with the same topology are compared, the Cu(I) development appears more evident for LL samples; this could be due to a more facile reactivity in the presence of multiple Cu(I) centres at a suitable distance for cooperative activation of O_2. The temperature at which the maximum Cu(I) development is detected before re-oxidation also appears slightly lower (350 °C) for the two LL materials with respect to the two HL ones (370-380 °C).
These XAS results are in good agreement with the temperature-dependent FTIR experiments previously reported for the HL Cu-CHA material during O_2 activation [42]. In the mentioned study, the characteristic IR band at ~ 3650 cm^{-1} assigned to the ν(O-H) vibration in redox-active Z[Cu(II)OH] species was observed to progressively decrease in intensity from 250 °C upwards. Connecting this line of evidence with the direct sensitivity to Cu oxidation state provided by XANES, it is likely that the same self-reduction mechanism observed in inert conditions also takes place in an oxidant environment, resulting in the transient formation of ZCu(I) species. Reaction between O_2 and these ZCu(I) species then represents a plausible pathway to form a variety of O_2-activated Cu(II) moieties, both mono- and multi-nuclear, including the active site for the MTM reaction.

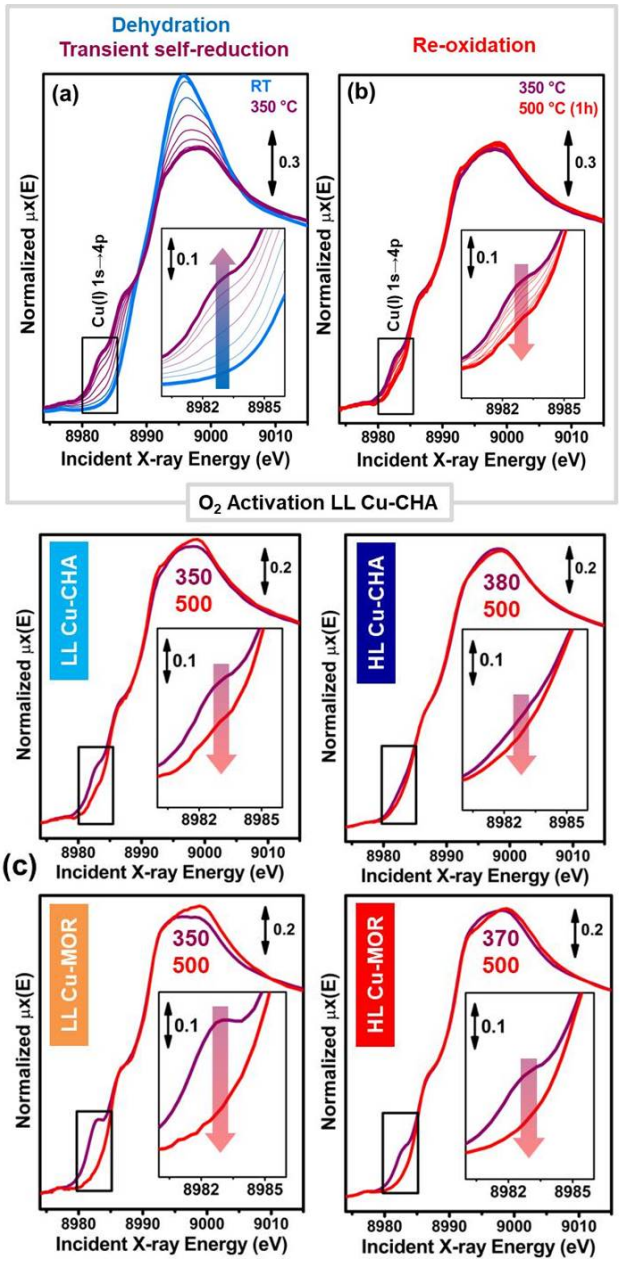

Figure 4. (a,b) Temperature/time dependent XANES spectra for a representative Cu-zeolite sample (LL Cu-CHA) collected during the O_2 activation step. Two phases can be identified: (a) dehydration and transient self-reduction up to 350 °C; (b) re-oxidation and stabilization from 350 °C upwards. (c) Comparison between the XANES scans showing the most developed Cu(I) fingerprint peak during the transient self-reduction phase of the O_2 activation step (purple lines) and the stable Cu(II) state reached after 1 h in O_2 at 500 °C (red lines) for all the investigated Cu-zeolites. In all the panels, the insets report a magnification of the rising-edge peak assigned to Cu(I) 1s →4p transitions.

3.4 Thermally-driven modifications in Cu-speciation after O_2 activation

The modifications in the Cu coordination and oxidation state were then measured while cooling the sample to 200 °C in O_2, and subsequently flushing in He at the same temperature (Figure 5). As we already noted in Section 3.2, both the 1s→3d pre-edge peak and the rising-edge region of the XANES confirm that the +2 oxidation state of Cu is not affected by the cooling step in O_2 and subsequent He flush. Nonetheless, while cooling, a progressive increase in the XANES WL region is detected, more pronounced for the two Cu-MOR materials, but also detectable in the Cu-CHA zeolites.

In parallel, a gradual increase in the intensity of the first-shell peak in the FT-EXAFS spectrum with respect to the O_2-activated state at 500 °C is recorded for all the samples. At 200 °C, the first-shell peak has increased of about 30% of its initial intensity at 500 °C, which is beyond what expected as a result of a decreased thermal

contribution to Debye-Waller (DW) factors [42]. The second-shell peak appear less perturbed, although some readjustments can be noted especially for the LL materials. This indicates that Cu ions maintain an equivalent coordination mode to the zeolite framework with respect to the O_2-activated state. The third maximum is only slightly perturbed, suggesting that multimeric species formed during high temperature treatment are structurally stable during the cooling step.

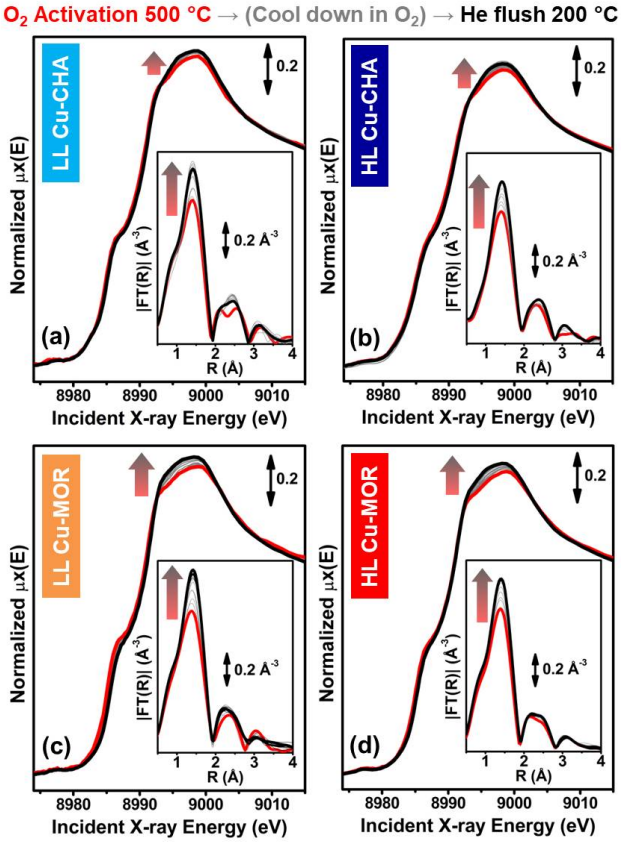

Figure 5. (a) Main panel: Temperature/time-dependent XANES spectra collected on LL Cu-CHA while cooling in O_2 from 500 to 200 °C before the subsequent He-flush at 200 °C. Inset: corresponding magnitude of the FT-EXAFS spectra. (b-d): as part (a) but for (b) HL Cu-CHA, (c) LL Cu-MOR, (d) HL Cu-MOR.

All these evidences, together with the EXAFS fitting results reported in Section 3.2, point to an average increase in the first-shell N_O coordination number of Cu while cooling in O_2, occurring in both Cu-CHA and Cu-MOR materials. Although a precise assignment is not straightforward due to the average character of the XAS technique, we suggest that this could be primarily due to a partial transition from end-on to side-on binding mode in mononuclear Cu(II)-superoxo adducts. This hypothesis is supported by Raman analysis of the O_2-activated HL Cu-CHA sample measured at RT [42], where the broad and intense bands at 1100 and 1155 cm^{-1} suggest the presence of Cu-superoxo species located at various Cu sites in both side-on and end-on binding modes [10, 32, 55].

3.5 CH_4 loading and CH_3OH extraction steps: average electronic and structural modifications of the Cu sites

Time-dependent XAS was then used to follow the evolution of Cu sites structure during the CH_4 loading step. Figure 6 reports a comparative overview of the resulting XANES (top panels) and FT-EXAFS (bottom panels) spectra for the investigated Cu-zeolites. As soon as the materials are exposed to CH_4, the characteristic Cu(I) peak at 8983 eV starts to develop, indicating the progressive formation of Cu(I) in agreement with several previous reports [3, 20, 42]. At the same time, the WL intensity decreases, suggesting that the newly formed Cu(I) species are characterized by a lower first-shell coordination number. The latter evidence is confirmed by

FT-EXAFS, showing a progressive decrease of the first-shell peak as a function of the contact time with CH_4. Overall, also the second- and third-shell maxima are slightly dampened, especially in LL samples, which points to rearrangements in the coordination mode to the framework and/or increased structural disorder in the Cu(I) component.

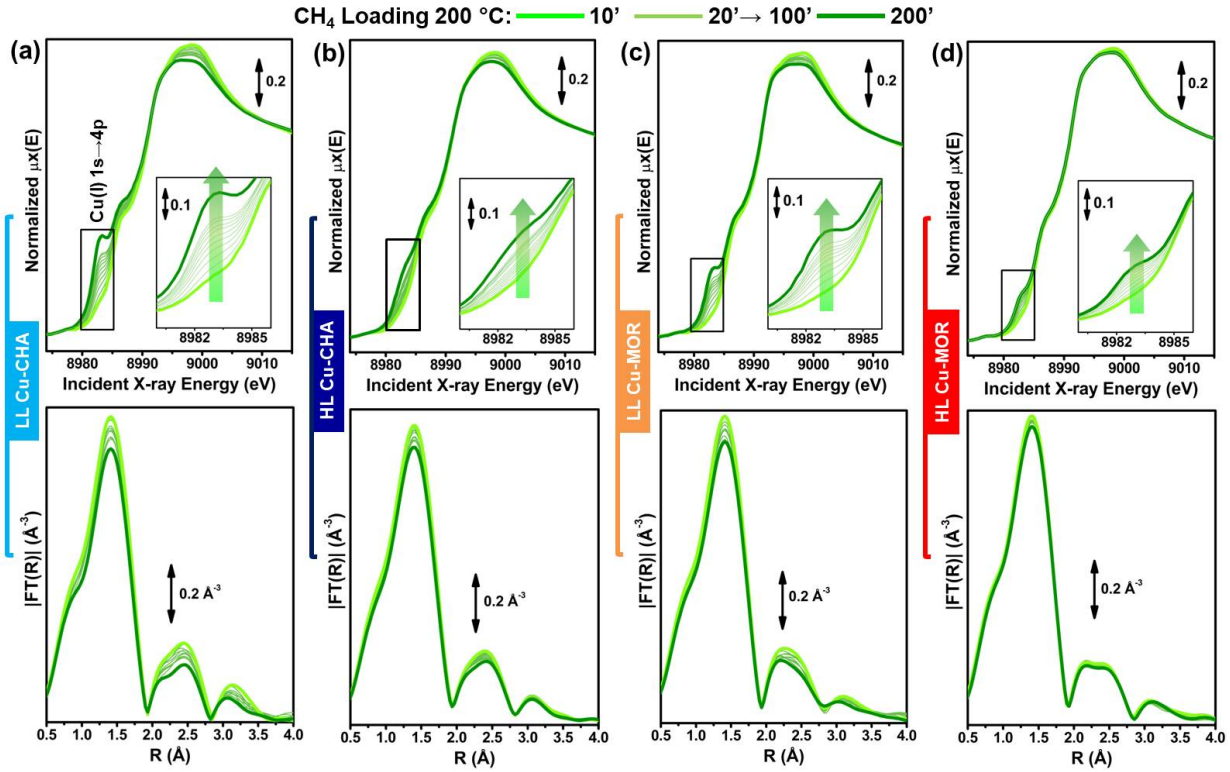

Figure 6. (a) Top panel: time-dependent XANES spectra collected on LL Cu-CHA at 200 °C in CH_4 from 10 to 200 min. The inset shows a magnification of the rising-edge peak assigned to Cu(I) 1s →4p transitions. Bottom panel: corresponding magnitude of the FT-EXAFS spectra. (b-d) As part (a) for (b) HL Cu-CHA; (c) LL Cu-MOR; (d) HL Cu-MOR.

Figure 7 compares the evolution of the normalized XANES intensity at 8983 eV as a function of time in CH_4 for the four Cu-zeolites. The increase of the 8983 eV peak and the decrease of the WL proceed always monotonically as a function of the exposure time. Nonetheless, their development rate is higher in the first 100 min in CH_4, whereas in the following 100 min smaller modifications are observed, almost undetectable in the case of HL Cu-MOR. Interestingly, these trends in the Cu(I) peak growth rate reflect the effect of increasing contact time during the CH_4 loading step on the productivity per Cu, previously reported for the HL Cu-CHA sample [42]. In particular, a substantial productivity increase was observed from 30 min (0.013 molCH_3OH/molCu) to 120 min (0.047 molCH_3OH/molCu); further increasing the contact time only resulted in a modest productivity rise, reaching a plateau at 0.058 molCH_3OH/molCu after ~300 min. Based on these evidences, the Cu(I) component formed upon interaction with CH_4 should include the progressively reacted Cu active sites. Indeed, reduction to Cu(I) is in line with different mechanisms proposed in the literature proposing the donation of an O_{ef} atom from active Cu-oxo species to the methyl moiety [45, 50, 51, 54], resulting into oxygenated intermediates strongly adsorbed at the active site.

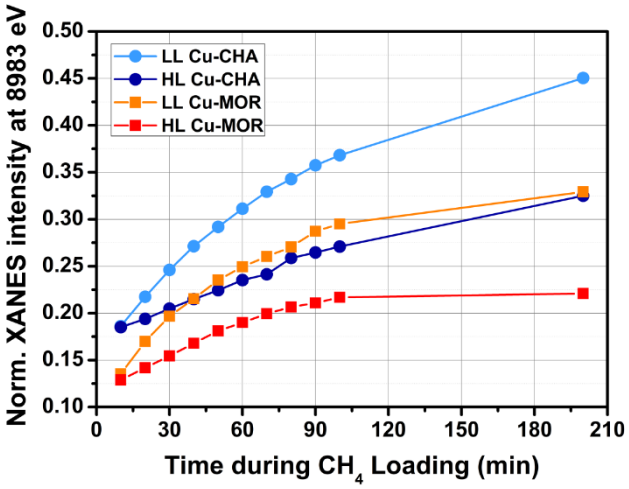

Figure 7. Evolution of the normalized XANES intensity of the Cu(I) fingerprint peak (8983 eV) as a function of time in CH_4 flow at 200 °C.

Nonetheless, it is clear that the maximum normalized intensity of the Cu(I) peak reached after 200 min in CH_4 does not correlate with the productivity of the investigated materials (see Figure 1 and Table S2). In particular, for the same framework topology, LL materials always show a significantly more pronounced Cu(I) 1s → 4p peak. Moreover, comparing samples with equivalent Cu-loading, the less productive Cu-CHA materials exhibit a higher Cu(I) peak with respect to the more productive Cu-MOR ones. A possible explanation could be a different coordination geometry for Cu(I) species formed in the different samples, known to significantly impact the intensity of the 1s → 4p transitions in the rising-edge region of the XANES, with linear species showing higher peaks with respect to bent ones [27, 49]. However, we note that the characteristic XAS features at the end of the CH_4 loading step (see also Figure 2) are remarkably similar in all the monitored Cu-zeolites. Hence, at least as a first approximation, we do expect Cu(I) species with quite similar coordination geometry, so that the intensity of the Cu(I) peak would be (qualitatively) representative of the relative abundance of Cu(I) moieties.

Under these assumptions, in both Cu-CHA and Cu-MOR the Cu(I) component developed after CH_4 interaction should also account for Cu-species which are inactive in the MTM process. These are Cu(II) moieties suggested to undergo reduction to Cu(I) while promoting unselective over-oxidation of CH_4 to CO_2 and CO. As a consequence, the total fraction of Cu(I) in the system at the end of the CH_4 loading step does not represent *tout-court* a good descriptor of the performance, since the response from the active sites is overshadowed by different processes, occurring at inactive Cu-species.

The complexity connected with the Cu(I) component formed during interaction with CH_4 is further highlighted by monitoring the subsequent steps of the process. Figure 8 shows the time-dependent XANES and FT-EXAFS spectra of the four samples during the CH_3OH extraction step, while fluxing 10% H_2O/He at 200 °C to enable the desorption of the intermediate species in the form of oxygenated products (i.e. CH_3OH and CH_3OCH_3). In all the cases, the final spectra collected at the end of the CH_4 loading step are reported for comparison, as green dashed lines. For the two LL samples, which showed a more pronounced development of the Cu(I) fingerprint peak in comparison with their HL counterparts, we have also collected XAS data at the end of the He flush performed prior to the extraction step (light grey dashed lines in Figure 8).

Strong similarities in the spectroscopic response of the four materials are observed also in this case. XAS reveals in all the cases the formation of hydrated Cu(II) species, characterized by an intense WL peak and a flat rising-edge region, similarly to what is observed for the as-prepared materials at RT before activation (see e.g. Figure 4a, blue curve). As discussed in Section 3.2, the contribution from hydrated Cu(II) species causes the progressive increase of the first-shell peak in the FT-EXAFS, together with the partial degradation of the second-shell maximum, testifying the mobilization of Cu ions [42] and possibly the hydrolysis of Cu-oxo clusters with Cu···Cu distances falling in that R-space range [20]. Hydrated Cu(II) quickly develops in all the

samples immediately after the admission of the steam flow. Most of the spectral changes are observed in the first 60 min of extraction shown in Figure 8, while at longer exposure to steam (up to 120 min) XAS remains substantially stable (see steady-state scans in Figure 2d).

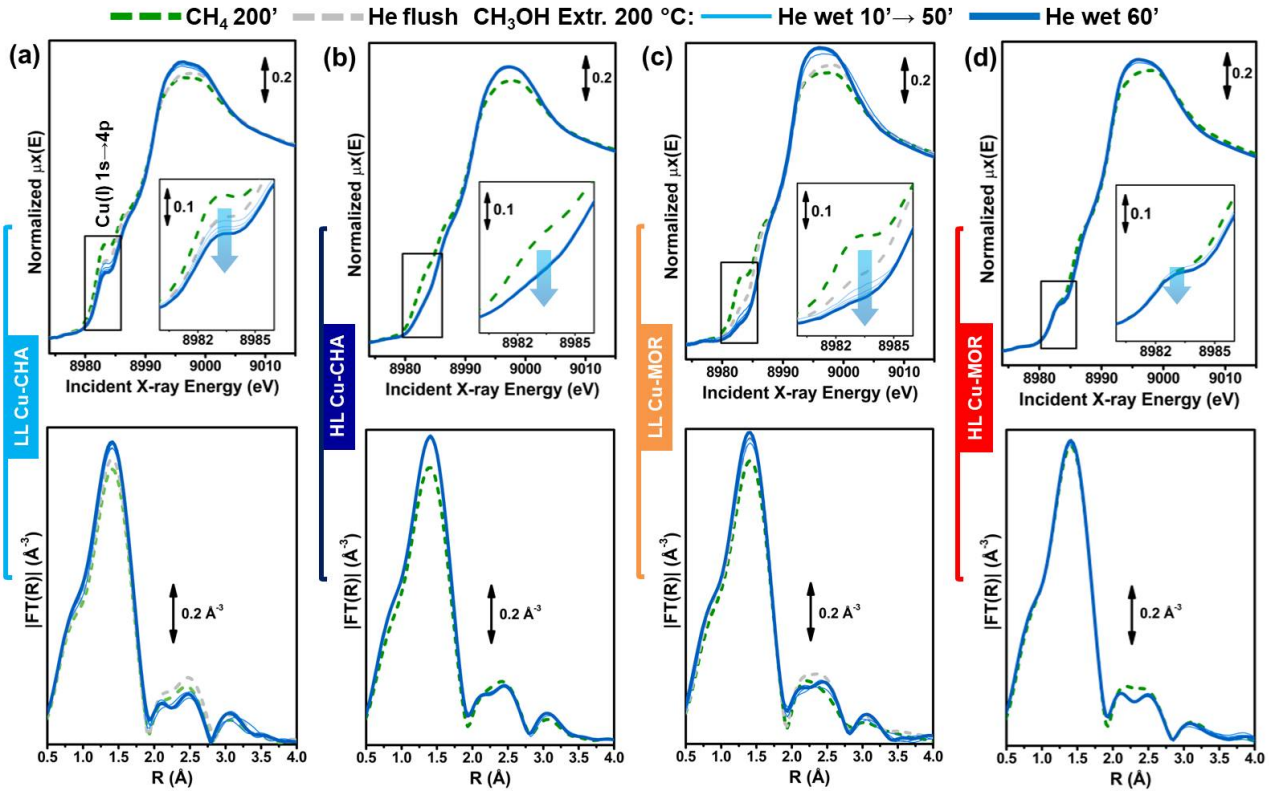

Figure 8. (a) Top panel: time-dependent XANES spectra on LL Cu-CHA during the CH_3OH extraction step at 200 °C (from 10 to 60 min). The inset shows a magnification of the rising-edge peak assigned to Cu(I) 1s →4p transitions. Bottom panel: corresponding magnitude of the FT-EXAFS spectra. (b-d) As part (a) for (b) HL Cu-CHA; (c) LL Cu-MOR; (d) HL Cu-MOR. For comparison, the XANES and FT-EXAFS spectra for each sample at the end of the CH_4 loading step (green dashed curves) are also reported. For LL materials, the XAS spectra collected after the He flush performed to remove unreacted CH_4 prior to CH_3OH extraction are also shown in parts (a) and (d) as grey dashed curves.

For all samples, steam contact causes a gradual decrease in the intensity of the Cu(I) fingerprint peak formed during interaction with CH_4. As evidenced in Figure 9, the effect is mostly pronounced for LL Cu-MOR and barely appreciable for HL Cu-MOR, while for two Cu-CHA samples we observe an intermediate intensity decrease. In LL Cu-CHA the Cu(I) peak is almost undetectable after 60 min of exposure to steam, and, based on both XANES and EXAFS features, the sample contains the highest fraction of hydrated Cu(II) among the investigated materials.

These XANES results suggest that steam admission to extract CH_3OH is accompanied by redox chemistry at the Cu sites, together with the hydration/mobilization phenomena discussed above. The recent report by Sushkevich et al. [50] proposes that H_2O itself can act as a mild oxidant for the stepwise MTM conversion. The authors designed an alternative protocol over Cu-MOR, which involves subsequent reaction cycles including activation in He at 400 °C followed by exposure to 7 bars of CH_4 at 200 °C and then H_2O/He while heating from 200 to 400 °C. Isotopic labelling experiments showed that during extraction, H_2O donates the O atom to regenerate Cu-oxo active centers in the zeolite, the same O atom which is then incorporated in the CH_3OH product desorbed at the following cycle.

Noticeably, the intensity decrease of the Cu(I) XANES fingerprint peak at 8983 eV during the extraction/regeneration step at 200 °C resembles what reported by Sushkevich et al. [50], notwithstanding the different experimental conditions. Nonetheless, it is interesting to note that a significant intensity decrease of this rising-edge peak is already observed for both the LL materials already while flushing with He the samples

after the CH_4 loading step, thus in the absence of H_2O (see grey dashed curves in Figure 8 and black arrows in Figure 9).

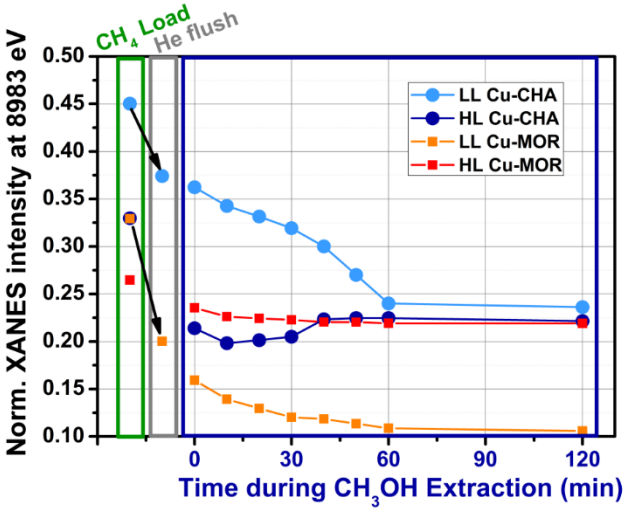

Figure 9. Evolution of the normalized XANES intensity of the Cu(I) fingerprint peak (8983 eV) as a function of time during the CH_3OH extraction step at 200 °C (blue box and time axis). For comparison, the value of the same parameter measured at the end of the CH_4 loading step (green box) and, for LL materials, the end of the He flush prior to CH_3OH extraction (grey box), are reported.

This behavior is quite interesting and would deserve further investigation in future studies. The preliminary observations obtained here for LL samples could point out to a redox equilibrium of certain (inactive) Cu species with CH_4-derived adducts, which restore their pristine 2+ oxidation state once CH_4 is removed from the reactor. Alternatively, both during He flush and interaction with steam during extraction, a readjustment in the average local environment of the metal centers could be invoked, resulting in a geometry-induced decrease of the Cu(I) 1s → 4p transition (e.g. due to modifications in the O_{fw}–Cu–O_{fw} bond angle) without an increase of the Cu(I) fraction in the system. Unfortunately, within the available data quality, it has not been possible to accurately quantify the background-subtracted intensity of the weak pre-edge peak at 8976 eV, fingerprinting the presence of d^9 Cu(II) ions. With this respect, the use of High Energy Resolution Fluorescence Detected (HERFD)-XANES [5, 16, 47] possibly in combination with other oxidation-state sensitive techniques (e.g. EPR) could provide additional insight.

4 Conclusions

In this contribution, XAS was employed to monitor the changes undergone by Cu sites in four Cu-CHA and Cu-MOR samples with low and high Cu loading (LL and HL, respectively), during the step-wise MTM process. Data were collected in steady-state conditions at the end of each key step (activation in O_2 at 500 °C, cooling down to 200 °C before flowing CH_4 and a He wet flow for products desorption) and during the different temperature ramps and isotherms. Moreover, the productivity of the set of samples was measured in independent experiments in order to get correlations between the structural and electronic information on Cu sites and their catalytic performance. Thus, CHA and MOR topologies treated in exactly the same conditions are here compared for the first time, in relation to the different catalytic activity and proposed structure of the active sites in these small and large pore zeolites [7].

This study allows to underline the potentialities and drawbacks of operando XAS. First, we were able to get some insights on the dynamic behaviour of the Cu species along the reaction, which could not be accessed by solely considering the final state of the materials. In particular, we observed for the first time a self-reduction of Cu(II) to Cu(I) while activating in O_2, pointing to the importance of the reaction between O_2 and Cu(I) at

relatively high temperature (< 350 °C) as a plausible pathway to form a variety of O_2-activated Cu(II) moieties, both mono- and multi-nuclear, including the active site for the MTM reaction. Indeed, the formation of active Cu-oxo species upon interaction of O_2 with Cu(I) sites formed by self-reduction has been studied in the literature by different groups [3, 42, 48]. These chemical steps have been pictorially depicted in Scheme 1, which has the main aim to resume some of the tentatively proposed structures observed by XAS in this work and reported in the literature. This includes the end-on and side-on mononuclear Cu(II)-superoxo adducts already proposed [42]. On the other hand, XAS is an element-selective but average technique, so that it is not straightforward to discriminate different contributions, especially in the EXAFS region. This limitation accounts for the difficulty in precisely defining the structure of the active sites in the presence of a mixture of Cu sites, as observed in this study.

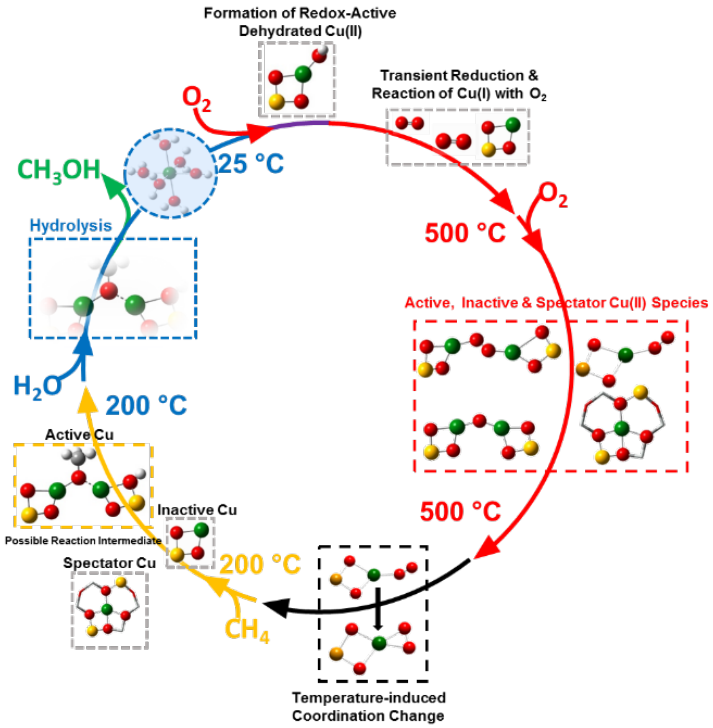

Scheme 1. Pictorial representation of some of the structures proposed in the literature (and tentatively assigned on the basis of the XAS data reported in this work), in the key steps of the MTM process.

Moreover, our time-resolved experiments, particularly concerning the CH_4 interaction and water assisted product formation/desorption, are in very good agreement with the reported influence of interaction time on the catalytic performance. Previous works [28, 42, 43] indicate that high-temperature O_2-activation guarantees a high population of active sites, and the 500 °C temperature employed here is indicated as an optimal value. Conversely, for the CH_4 loading step the best performance in terms of both productivity and selectivity requires a lower temperature: 200 °C in the case of Cu-CHA [42]. Our experiments showed how the temperature change (and subsequent He flush) did not affect the Cu coordination mode to the zeolite framework and the stability of multimeric structures, while modifying the coordination of the oxo extra-ligand to Cu (partial transition from end-on to side-on binding mode). On the other hand, the reduction to Cu(I) during CH_4 flow is in line with different mechanisms proposed in the literature proposing the donation of an O_{ef} atom from active Cu-oxo species to the methyl moiety [45, 50, 51, 54], resulting into oxygenated intermediates strongly adsorbed at the active site, as exemplified in Scheme 1.

It is important to point out that these results are not conclusive, since they are not able to explain the higher catalytic activity reported for Cu-MOR with respect to Cu-CHA catalysts. Indeed, the observed fingerprints are very similar for all samples in all the steps, excepted for small differences described in the text. This suggests that the local coordination of Cu sites is similar on average on the different topologies, so that the

different activity could be ascribed to second-sphere effects (i.e. the zeolite lattice acting as the active pocket of a metalloenzyme [53], or to a more uniform distribution of Cu as active sites in the MOR framework [19, 20]. Similarly, the role played by water in the process (whether it plays an active role in the catalysis or it is simply used to expel oxidation products from the chemisorbed positions and recover the initial state of the catalyst) is still an open and intriguing question.

As a final remark, it is very tempting to try a comparison between the active sites structure and related mechanisms studied on Cu-zeolites and those connected to Fe-zeolites, able to selectively form methanol from methane using H_2O_2. This is a very fascinating subject, with many complexity degrees in relation to the different reaction media (gas *vs* liquid phase) and different chemistry of the involved transition metal ions. These are well known to show a similar redox activity (*i.e.* Cu(II)/Cu(I) *vs* Fe(III)/Fe(II) reversible cycles) and tendency to form binuclear oxo-compounds, in both enzymes or homogeneous complexes. In particular, both metal ions are present as active sites in monooxygenase enzymes: while binuclear Fe cores are well established for methane monooxygenase MMO, the discussion about the nuclearity of active sites in *particulate* methane monooxygenase pMMO is still ongoing, leaving a lot of space for research in this intriguing field of chemistry.

Acknowledgments

EB acknowledges Innovation Fund Denmark (Industrial postdoc n. 5190-00018B). DKP, MD acknowledge iCSI Centre for Research based Innovation receiving financial support from the Research Council of Norway (contract no 237922). We are deeply indebted with S. Bordiga, C. Lamberti, S. Svelle, P. Beato, for insightful discussions and support to the whole research project. We also acknowledge C. Lamberti and I. A. Pankin for their help during the XAS measurements, A. Marsicano for her help in the XAS data analysis, and S. Teketel for the synthesis of the Cu-CHA samples. We are grateful to A. Longo for the friendly and competent support during XAS data acquisition on the BM26A beamline of the ESRF.

References

[1] E.M. Alayon, M. Nachtegaal, A. Bodi, M. Ranocchiari, J.A. van Bokhoven, Phys. Chem. Chem. Phys. 17 (2015) 7681-7693.

[2] E.M. Alayon, M. Nachtegaal, M. Ranocchiari, J.A. van Bokhoven, Chem. Comm. 48 (2012) 404-406.

[3] E.M.C. Alayon, M. Nachtegaal, A. Bodi, J.A. van Bokhoven, ACS Catal. 4 (2014) 16-22.

[4] S.A. Bates, A.A. Verma, C. Paolucci, A.A. Parekh, T. Anggara, A. Yezerets, W.F. Schneider, J.T. Miller, W.N. Delgass, F.H. Ribeiro, J. Catal. 312 (2014) 87-97.

[5] M. Bauer, Phys. Chem. Chem. Phys. 16 (2014) 13827-13837.

[6] D. Bellet, B. Gorges, A. Dallery, P. Bernard, E. Pereiro, J. Baruchel, J. Appl. Crystallogr. 36 (2003) 366-367.

[7] G. Berlier, V. Crocellà, M. Signorile, E. Borfecchia, F. Bonino, S. Bordiga, Characterization of Metal Centers in Zeolites for Partial Oxidation Reactions, Structure and Bonding, Springer, Berlin, Heidelberg, 2018, pp. 1-64.

[8] G. Berlier, G. Spoto, S. Bordiga, G. Ricchiardi, P. Fisicaro, A. Zecchina, I. Rossetti, E. Selli, L. Forni, E. Giamello, C. Lamberti, J. Catal. 208 (2002) 64-82.

[9] E. Borfecchia, K.A. Lomachenko, F. Giordanino, H. Falsig, P. Beato, A.V. Soldatov, S. Bordiga, C. Lamberti, Chem. Sci. 6 (2015) 548-563.

[10] P. Chen, D.E. Root, C. Campochiaro, K. Fujisawa, E.I. Solomon, J. Am. Chem. Soc. 125 (2003) 466-474.

[11] K.A. Dubkov, N.S. Ovanesyan, A.A. Shteinman, E.V. Starokon, G.I. Panov, J. Catal. 207 (2002) 341-352.

[12] M.M. Forde, R.D. Armstrong, R. McVicker, P.P. Wells, N. Dimitratos, Q. He, L. Lu, R.L. Jenkins, C. Hammond, J.A. Lopez-Sanchez, C.J. Kiely, G.J. Hutchings, Chem. Sci. 5 (2014) 3603-3616.

[13] H. Funke, A.C. Scheinost, M. Chukalina, Phys. Rev. B 71 (2005) 7.

[14] F. Gao, N.M. Washton, Y.L. Wang, M. Kollar, J. Szanyi, C.H.F. Peden, J. Catal. 331 (2015) 25-38.

[15] F. Giordanino, E. Borfecchia, K.A. Lomachenko, A. Lazzarini, G. Agostini, E. Gallo, A.V. Soldatov, P. Beato, S. Bordiga, C. Lamberti, J. Phys. Chem. Lett. 5 (2014) 1552-1559.

[16] P. Glatzel, U. Bergmann, Coord. Chem. Rev. 249 (2005) 65-95.
[17] M.H. Groothaert, P.J. Smeets, B.F. Sels, P.A. Jacobs, R.A. Schoonheydt, J. Am. Chem. Soc. 127 (2005) 1394-1395.
[18] M.H. Groothaert, J.A. van Bokhoven, A.A. Battiston, B.M. Weckhuysen, R.A. Schoonheydt, J. Am. Chem. Soc. 125 (2003) 7629-7640.
[19] S. Grundner, W. Luo, M. Sanchez-Sanchez, J.A. Lercher, Chem. Comm. 52 (2016) 2553-2556.
[20] S. Grundner, M.A. Markovits, G. Li, M. Tromp, E.A. Pidko, E.J. Hensen, A. Jentys, M. Sanchez-Sanchez, J.A. Lercher, Nat. Commun. 6 (2015) 7546.
[21] C. Hammond, N. Dimitratos, R.L. Jenkins, J.A. Lopez-Sanchez, S.A. Kondrat, M.H. ab Rahim, M.M. Forde, A. Thetford, S.H. Taylor, H. Hagen, E.E. Stangland, J.H. Kang, J.M. Moulijn, D.J. Willock, G.J. Hutchings, ACS Catal. 3 (2013) 689-699.
[22] C. Hammond, N. Dimitratos, J.A. Lopez-Sanchez, R.L. Jenkins, G. Whiting, S.A. Kondrat, M.H. ab Rahim, M.M. Forde, A. Thetford, H. Hagen, E.E. Stangland, J.M. Moulijn, S.H. Taylor, D.J. Willock, G.J. Hutchings, ACS Catal. 3 (2013) 1835-1844.
[23] C. Hammond, M.M. Forde, M.H. Ab Rahim, A. Thetford, Q. He, R.L. Jenkins, N. Dimitratos, J.A. Lopez-Sanchez, N.F. Dummer, D.M. Murphy, A.F. Carley, S.H. Taylor, D.J. Willock, E.E. Stangland, J. Kang, H. Hagen, C.J. Kiely, G.J. Hutchings, Angew. Chem. Int. Ed. Engl. 51 (2012) 5129-5133.
[24] C. Hammond, I. Hermans, N. Dimitratos, ChemCatChem 7 (2015) 434-440.
[25] B. Ipek, M.J. Wulfers, H. Kim, F. Göltl, I. Hermans, J.P. Smith, K.S. Booksh, C.M. Brown, R.F. Lobo, ACS Catal. 7 (2017) 4291-4303.
[26] T.V.W. Janssens, H. Falsig, L.F. Lundegaard, P.N.R. Vennestrøm, S.B. Rasmussen, P.G. Moses, F. Giordanino, E. Borfecchia, K.A. Lomachenko, C. Lamberti, S. Bordiga, A. Godiksen, S. Mossin, P. Beato, ACS Catal. 5 (2015) 2832-2845.
[27] L.S. Kau, D.J. Spirasolomon, J.E. Pennerhahn, K.O. Hodgson, E.I. Solomon, J. Am. Chem. Soc. 109 (1987) 6433-6442.
[28] Y. Kim, T.Y. Kim, H. Lee, J. Yi, Chem. Commun. 53 (2017) 4116-4119.
[29] C. Lamberti, S. Bordiga, M. Salvalaggio, G. Spoto, A. Zecchina, F. Geobaldo, G. Vlaic, M. Bellatreccia, J. Phys. Chem. B 101 (1997) 344-360.
[30] S.C. Larsen, A. Aylor, A.T. Bell, J.A. Reimer, J. Phys. Chem. 98 (1994) 11533-11540.
[31] K.A. Lomachenko, E. Borfecchia, C. Negri, G. Berlier, C. Lamberti, P. Beato, H. Falsig, S. Bordiga, J. Am. Chem. Soc. 138 (2016) 12025-12028.
[32] D. Maiti, H.C. Fry, J.S. Woertink, M.A. Vance, E.I. Solomon, K.D. Karlin, J. Am. Chem. Soc. 129 (2007) 264-265.
[33] A. Martini, E. Borfecchia, K.A. Lomachenko, I.A. Pankin, C. Negri, G. Berlier, P. Beato, H. Falsig, S. Bordiga, C. Lamberti, Chem. Sci. 8 (2017) 6836-6851.
[34] M. Munoz, P. Argoul, F. Farges, Am. Miner. 88 (2003) 694-700.
[35] K. Narsimhan, K. Iyoki, K. Dinh, Y. Roman-Leshkov, ACS Cent. Sci. 2 (2016) 424-429.
[36] S. Nikitenko, A.M. Beale, A.M.J. van der Eerden, S.D.M. Jacques, O. Leynaud, M.G. O'Brien, D. Detollenaere, R. Kaptein, B.M. Weckhuysen, W. Bras, J. Synchrot. Radiat. 15 (2008) 632-640.
[37] G.A. Olah, A. Goeppert, M. Czaun, T. Mathew, R.B. May, G.K. Prakash, J. Am. Chem. Soc. 137 (2015) 8720-8729.
[38] G.T. Palomino, P. Fisicaro, S. Bordiga, A. Zecchina, E. Giamello, C. Lamberti, J. Phys. Chem. B 104 (2000) 4064-4073.
[39] G.I. Panov, A.S. Kharitonov, V.I. Sobolev, 98 (1993) 1-20.
[40] C. Paolucci, J.R. Di Iorio, F.H. Ribeiro, R. Gounder, W.F. Schneider, 59 (2016) 1-107.
[41] C. Paolucci, A.A. Parekh, I. Khurana, J.R. Di Iorio, H. Li, J.D. Albarracin Caballero, A.J. Shih, T. Anggara, W.N. Delgass, J.T. Miller, F.H. Ribeiro, R. Gounder, W.F. Schneider, J. Am. Chem. Soc. 138 (2016) 6028-6048.
[42] D.K. Pappas, E. Borfecchia, M. Dyballa, I.A. Pankin, K.A. Lomachenko, A. Martini, M. Signorile, S. Teketel, B. Arstad, G. Berlier, C. Lamberti, S. Bordiga, U. Olsbye, K.P. Lillerud, S. Svelle, P. Beato, J. Am. Chem. Soc. 139 (2017) 14961-14975.
[43] M.B. Park, S.H. Ahn, A. Mansouri, M. Ranocchiari, J.A. van Bokhoven, ChemCatChem 9 (2017) 3705-3713.
[44] B. Ravel, M. Newville, J. Synchrotron Radiat. 12 (2005) 537-541.

[45] M. Ravi, M. Ranocchiari, J.A. van Bokhoven, Angew. Chem. Int. Edit. (2017) in press, doi: 10.1002/anie.201702550.
[46] M. Sano, S. Komorita, H. Yamatera, Inorg. Chem. 31 (1992) 459-463.
[47] J. Singh, C. Lamberti, J.A. van Bokhoven, Chem. Soc. Rev. 39 (2010) 4754-4766.
[48] P.J. Smeets, R.G. Hadt, J.S. Woertink, P. Vanelderen, R.A. Schoonheydt, B.F. Sels, E.I. Solomon, J. Am. Chem. Soc. 132 (2010) 14736-14738.
[49] E.I. Solomon, D.E. Heppner, E.M. Johnston, J.W. Ginsbach, J. Cirera, M. Qayyum, M.T. Kieber-Emmons, C.H. Kjaergaard, R.G. Hadt, L. Tian, Chem. Rev. 114 (2014) 3659-3853.
[50] V.L. Sushkevich, D. Palagin, M. Ranocchiari, J.A. van Bokhoven, Science 356 (2017) 523-527.
[51] P. Tomkins, M. Ranocchiari, J.A. van Bokhoven, Acc. Chem. Res. 50 (2017) 418-425.
[52] M.-L. Tsai, R.G. Hadt, P. Vanelderen, B.F. Sels, R.A. Schoonheydt, E.I. Solomon, J. Am. Chem. Soc. 136 (2014) 3522-3529.
[53] P. Vanelderen, B.E. Snyder, M.L. Tsai, R.G. Hadt, J. Vancauwenbergh, O. Coussens, R.A. Schoonheydt, B.F. Sels, E.I. Solomon, J. Am. Chem. Soc. 137 (2015) 6383-6392.
[54] P. Vanelderen, J. Vancauwenbergh, B.F. Sels, R.A. Schoonheydt, Coord. Chem. Rev. 257 (2013) 483-494.
[55] J.S. Woertink, P.J. Smeets, M.H. Groothaert, M.A. Vance, B.F. Sels, R.A. Schoonheydt, E.I. Solomon, P. Natl. Acad. Sci. USA. 106 (2009) 18908-18913.
[56] M.J. Wulfers, S. Teketel, B. Ipek, R.F. Lobo, Chem. Comm. 51 (2015) 4447-4450.